24th COBEM - 2017

24th ABCM International Congress of Mechanical Engineering
December 3-8, 2017, Curitiba, PR, Brazil

COBEM2017-0541

CHARACTERIZATION OF SLUG FLOW IN ANNULAR DUCT, USING HIGH SPEED VIDEO CAMERA, ANNULAR WIRE-MESH SENSOR AND PIV

Marlon M Hernández Cely
Victor E. C. Baptistella
Oscar M. H. Rodriguez.
Industrial Multiphase Flow Laboratory-LEMI, Mechanical Engineering Department, São Carlos School of Engineering, University of São Paulo (USP), São Carlos, SP, Brazil
marlonhc@usp.br
victor.baptistella@usp.br
oscarmhr@sc.usp.br

Abstract. *An experimental study is presented where air-water two-phase flow is studied in an annular duct with an external diameter of 155 mm, an inner diameter of 60 mm and 10.5 m long. The Fast Fourier transform (FFT) is used to calculate the power spectral density (PSD) obtained from the time signal of void fraction measured by a home-made Annular Wire-Mesh Sensor (AWMS). The average velocity of the bubble is estimated using high-speed video recording. The bubble velocity data are compared with the velocity data obtained by Particle Image Velocimetry (PIV) together with the AWMS.*

Keywords: *two-phase flow, PSD, annular duct, air-water flow, AWMS, PIV.*

1. INTRODUCTION

Gas-liquid flows in annular ducts are present in many industrial applications, for example in directional oil wells. However, there are few studies on characterization and analysis of geometrical and kinematic properties of two-phase air-water flows in big annular ducts. The goal is the analysis of frequency of passage of bubbles in slug flow and void fraction. It is used the Fast Fourier Transform (FFT) to calculate the Power Spectral Density (PSD) obtained from the time signal of void fraction measured by the annular wire-mesh sensor (AWMS). The average velocity of the bubble is calculated using high-speed video recording and compared with the velocity data obtained by particle image velocimetry (PIV) together with AWMS.

Jones and Zuber (1975) showed that the probability density function (PDF) of the void-fraction fluctuations may be used as an objective and quantitative flow-pattern discriminator for the three dominant flow patterns, bubbly, slug, and annular flow. Takeda (1995), using the pulsed ultrasonic echography together with the detection of the instantaneous Doppler shift frequency where the position-averaged power spectrum and the time-averaged energy spectral density were used to study the dynamic characteristics of the flow. Fulgosi et al. (2003), analyzed the turbulent kinetic energy and Reynolds stress and revealed that the interface deformations mainly affect the so-called boundary term involving the redistribution of energy, i.e., by the action of pressure. A similar type of relationship is found between the correlation entropy and the spectral entropy of pressure time series measured in fluidized beds, according to van der Schaaf et al. (2004), spectral analysis, most often the PSD function, was quantified.

The WMS was first described by Johnson (1987), as an intrusive sensor for measuring the fraction of water in oil, based on fluid conductivity. Prasser et al. (1998) ensured the elimination of crosstalk between the electrodes and the WMS was developed for application in nuclear power plants, in which water-steam flow is subjected to high temperatures and pressures. Silva et al.(2007) developed a WMS based on the permittivity of the fluid, which expands the range of substances that can be identified. Also, the technology has been applied in sensors of several different shapes Damsohn and Prasser, (2009a), Damsohn and Prasser (2009b), Belt et al. (2010), and Höhne et al. (2006), but the operation principle and the associated electronic circuits are still the same. A comprehensive review of the literature was carried out by Velasco Peña and Rodriguez (2015), with relevant and recent implementations, remarkably in gas-liquid and liquid-liquid flows, comparing it with other techniques. In addition, it is shown how the sensor can be adapted to each application and its different geometries, pointing out its flexibility.

The novelty of this work is the use of a WMS sensor in an annular duct with the help of high-speed video recording and PIV to measure void fraction as a function of time and, after calculating the PSD, to obtain frequency of passage and velocity of bubbles in slug flow.

2. AWMS OPERATING PRINCIPLE

An annular wire-mesh sensor (AWMS) is essentially made of two plane arrays of wire electrodes (transmitter and receiver wires) which make an angle of 90° with respect to each other (Fig. 1a and 1b). The prototype used in the experiments was designed and constructed in the Industrial Multiphase Flow Laboratory (LEMI), USP, Brazil, and it consists of a 16 x 16 wire grid. The axial spacing of the wire planes is 1.4 mm and each wire is 9.6875 mm apart from another one (see details of the sensor and installation in Fig. 1a and b). The sensor was installed in an annular duct with an external diameter of 155 mm and an inner diameter of 60 mm, the wires are made from 316 stainless steel with a diameter of 0.2 mm, so the sensor has an intrusiveness factor of 4.08% (Fig.1a). The sensor was designed to get the scans of the cross section of the outer annular duct installation called " Inverted Shroud Separator", present in the core of Thermal and fluid Engineering. The wires of each plane form a mesh of electrodes, in each electrode, or crossing point between wires, is measured the complex permittivity of the fluid flowing through the sensor, which is equivalent to measuring the electrical resistance and capacitance, simultaneously. Each transmitter wire (red) is activated in sequence and sends an electrical signal through the fluid; thus, each receiver wire (blue) carries a signal containing the information to identify the characteristics of the fluids present at each crossing point (Fig.1a). Non-active transmitters are grounded. Activating the last transmitter wire, a full data set about the type of fluid or phase fractions into the entire cross section is obtained. From this information, it is possible to obtain local mean fractions across the section over time, phase distributions along the section, in-situ void fraction and 3D images of the flow.

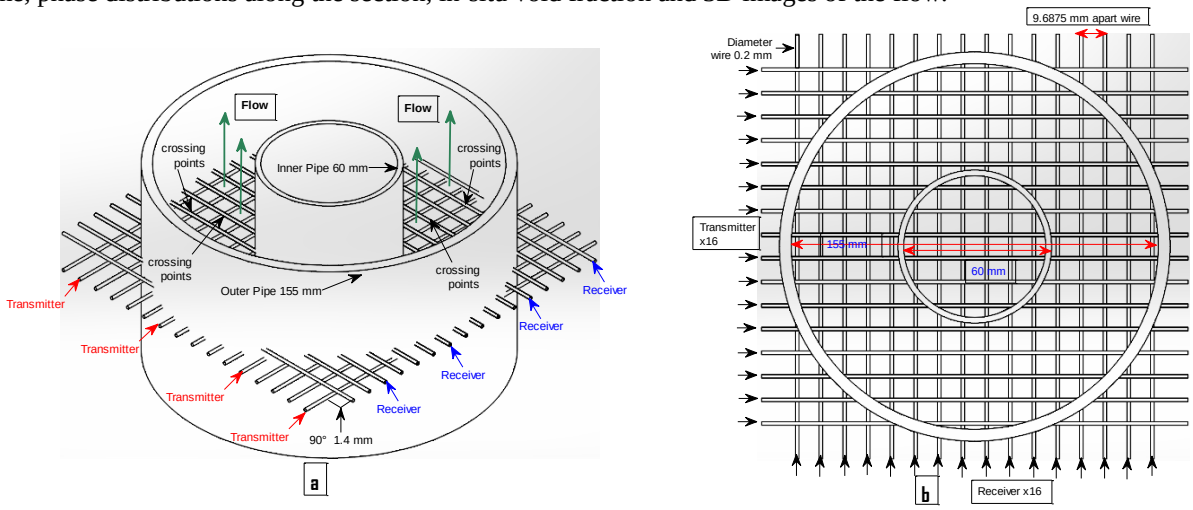

Figure 1a and 1b. Schematic representation of the Annular Wire-Mesh Sensor (AWMS), with its location in an annular duct.

To measure the electrical admittance of fluid an autobalanced-bridge circuit is used. Fig. 2 shows a general diagram of the circuit. In this Fig. 2, Y_f and Y_x are feedback and fluid admittance, respectively, V_i is the excitation signal and V_o is the output signal. Note that the AWMS and a transimpedance amplifier form the autobalanced-bridge circuit. This circuit has a voltage gain defined by Eq. (1):

$$A_V = {V_o}/{V_i} = -{Y_x}/{Y_f} \tag{1}$$

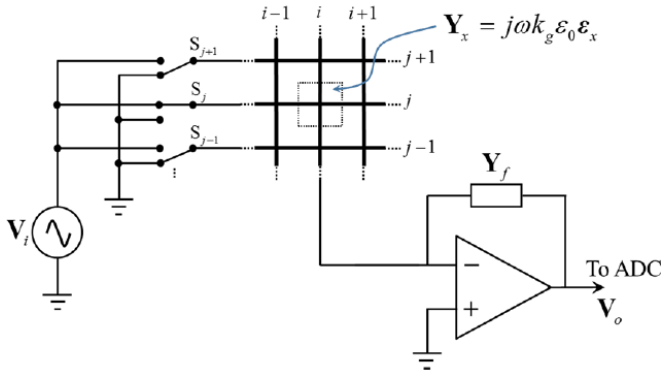

Figure 2. General circuit diagram for measurement of complex permittivity using annular wire-mesh sensor (Velasco Peña and Rodriguez (2015)).

3. EXPERIMENTAL SETUP AWMS

Figgure 3 provides an overview of the experimental apparatus containing a robust inclinable steel beam 11m long, 60 cm high and 40 cm wide that can be inclined from 0 to 90 degrees from horizontal. On the steel beam it is installed the test section with 10.5 m long. The test section is formed by two concentrically assembled pipes, the external and internal pipes are made of borosilicate glass and PVC, respectively. A by-pass line allows the usage of the quick-closing-valve (QCV) technique to measure the in-situ void fraction. The water is kept in polyethylene tanks. The air is stored in a pressurized tank. A compressor fills the air tank and the air flow is controlled by electromechanical valves. Positive displacement water pump, controlled by variable-frequency drivers, pumps the phase to the test line. Water and air are joined at the beginning of the test section. Positive displacement and vortex flow meters are used to measure the flow rates of the fluids. An annular wire-mesh sensor (AWMS) is used to obtain the phase fraction, distribution and cross-sectional images of the flow. A lateral view of the flow is recorded using a HSC (Olympus i-Speed 3, monochrome).

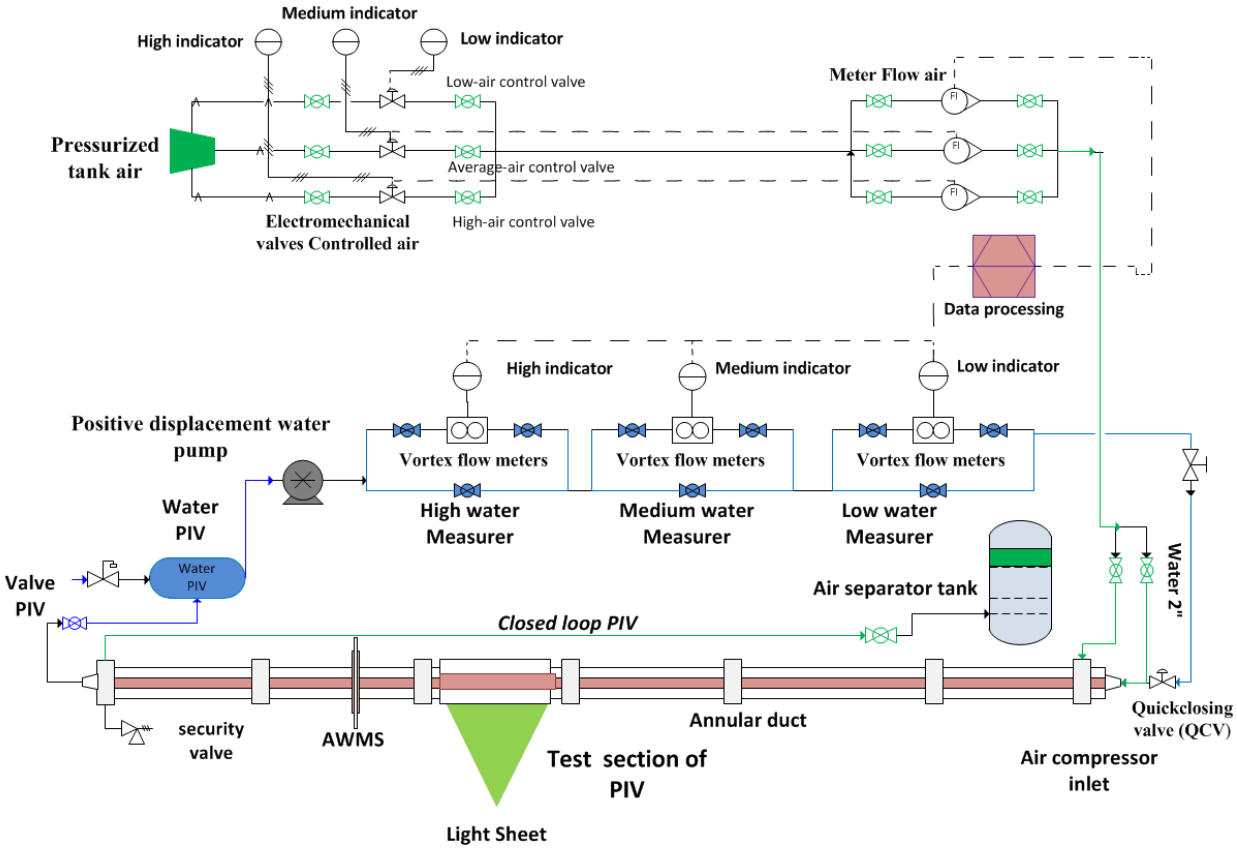

Figure 3. Experimental Apparatus AWMS and PIV.

3. 4. DATA REDUCTION AND PROCESSING

Fig. 4 shows void fraction data for five different flow conditions, keeping the water superficial velocity at 0.092 m/s and changing the air superficial velocity from 0.042 to 0.055 m/s. During the AWMS data treatment, we tested 12 different permittivity models to relate local phase fraction and the measured local electrical permittivity. By comparison with data obtained via quick-closing valves, four permittivity models were selected. The Bruggeman model was chosen, Eq.(2), because within the range of flow rates tested in this work it gave the best results in comparison with the quick-closing valves measurements.

$$\alpha = \frac{(\varepsilon_x + \varepsilon_2)(\varepsilon_x - \varepsilon_1)}{\varepsilon_x(\varepsilon_2 - \varepsilon_x)} \tag{2}$$

where α is the void fraction, ε_x, ε_2 and ε_1 are mixture, air and water permittivity, respectively.

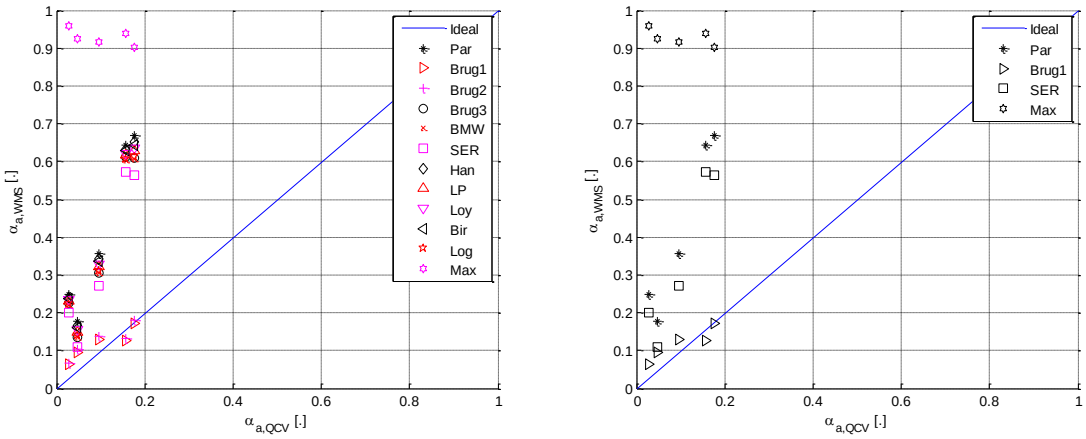

Figure 4. Comparison of void fraction ($\boldsymbol{\alpha}$) measurements via AWMS and quick-closing-valve technique, J_w = 0.092 m/s and different air superficial velocities. Left figure, 12 different permittivity models. Right figure the 4 selected models.

Power spectral density PSD, provides very valuable information on the internal dynamics of the flow, in this case, the frequency of passage of the bubble and the void-fraction present in the flow of the annular duct. It describes how the energy of a signal or a time series is distributed with frequency.

When the energy of the signal is concentrated around a finite time interval, Fig. 5, especially if its total energy is finite, one may compute the energy spectral density. More commonly used is the power spectral density (or simply power spectrum), which applies to signals existing over all time, Fig. 6, or over a time period large enough (especially in relation to the duration of a measurement) that it could as well have been over an infinite time interval. The spectrum of a physical process (multiphase flow) often contains essential information about the nature of it. Obtaining a spectrum from time series, Fig. 5, involves the Fourier transform, and generalizations based on Fourier analysis.

One can see in Fig. 5 the PSD based on void-fraction time signal, obtained by the AWMS using the Bruggeman model. The frequency is normalized by ($\pi * f_{sample} / 2\pi$), where f_{sample}, in this case, was 100 Hz. The results will be commented in the next section. In Fig. 6, the void fraction signal presents 32 peaks, corresponding to 32 bubbles, a frequency of 32/30 bubbles/second, equivalent to 1.067 Hz and a mean value of 0.096. Fig. 7 shows a square wave obtained from the data of fig. 6, it was useful in the determination of the bubble length. To obtain the square wave, a single crossing point of the AWMS was used, simulating a single probe, so it could be easily seen where the bubble started and where it ended. These points are not clear in fig. 6, due to the fact that if a single crossing point measures air, while the rest measures water, the void fraction will be insignificant and the point will not be taken as the beginning of the bubble (or the ending).

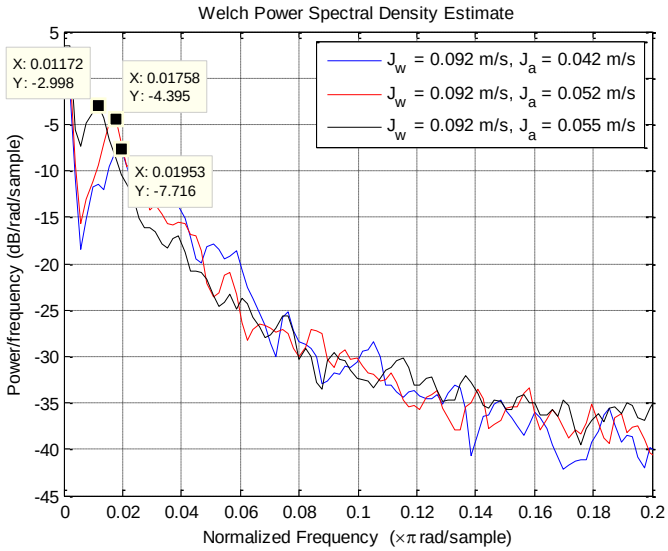

Figure 5. Power Spectral Density, estimated for different superficial velocities.

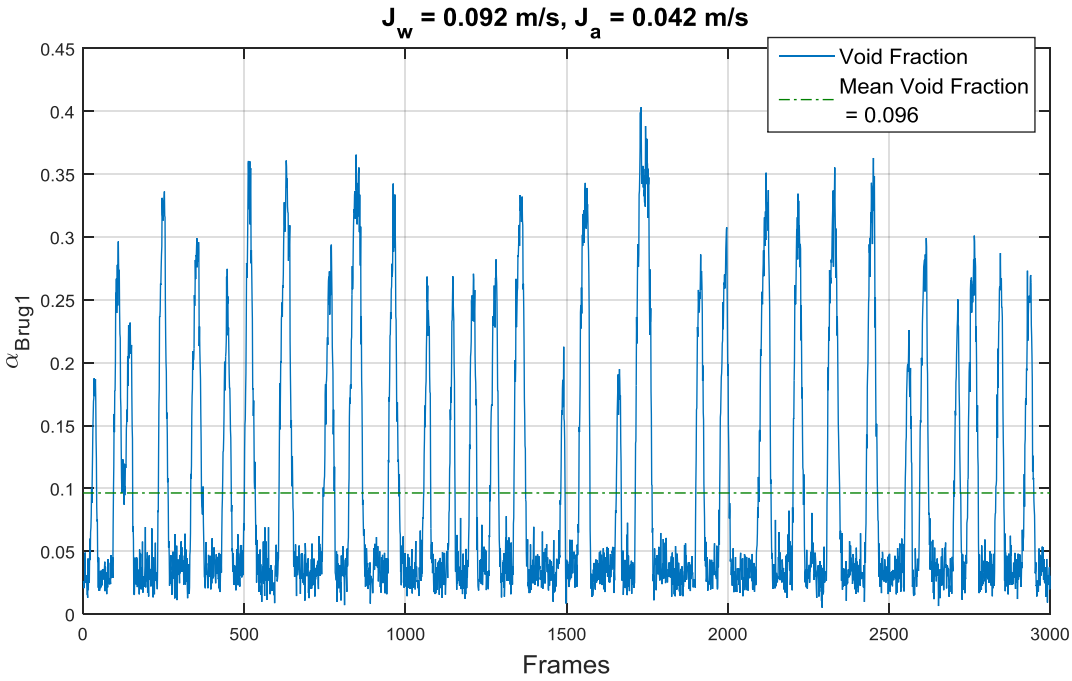

Figure 6. Void-fraction time signal for J_w = 0.092 m/s and J_a = 0.042 m/s, in 3000 frames.

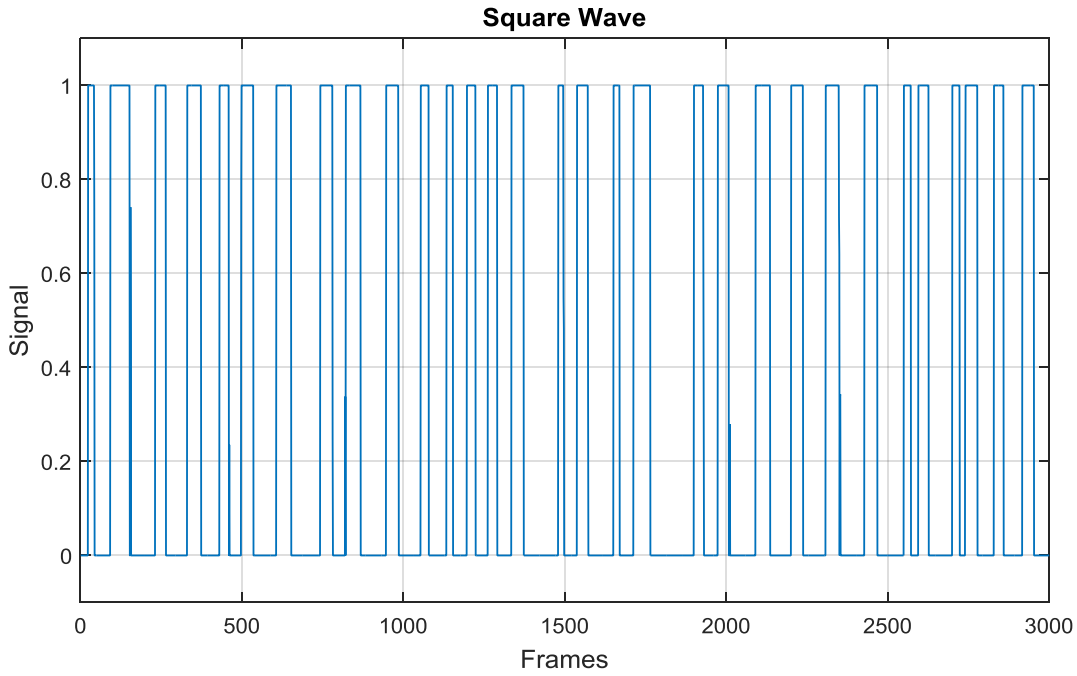

Figure 7. Square wave for J_w = 0.092 m/s and J_a = 0.042 m/s, in 3000 frames.

Two techniques were applied for the bubble velocity analysis:

I. Measuring the velocity of passage of a bubble using the high speed video camera. The video is observed and then measured how many frames the bubble took to pass through the visualization box, which measures 47.5 cm. Saving the time, calculated according to the relationship 0.01 frames/second, the velocity is calculated with Eq.(3).

$$V_{HSVC} = \frac{L_{box}}{t_{box}} \tag{3}$$

where V_{HSVC} = velocity given by high-speed video camera, L_{box} = visualization-box length (47.5 cm) and t_{box} = time of crossing the visualization box (0.01 frames/second).

II. Calculating the velocity based on the data of the AWMS. We have to first calculate how many frames are needed for the bubble to pass the cross section of the sensor and apply the relation 0.01 frames / second, with which we obtain the time. To calculate the distance it is used the mean bubble length that was measured by the PIV Images. Applying both to Eq.(4), gives velocity.

$$V_{WMS} = \frac{L_{bubble}}{t_{bubble}} \tag{4}$$

where V_{WMS} = velocity by wire-mesh sensor, L_{bubble} = bubble length (given by PIV images) and t_{bubble} = time to cross the wire-mesh sensor (0.01 frames/second).

5. RESULTS

One can see in Fig. 5 that the dominant bubble-passage frequency diminishes with increasing the air flow rate. This result can be explained by the higher void fraction that would result in bigger bubbles due to more intense bubble coalescence. In addition, the power peaks were intensified when the frequency decreased. Similar results are found in the literature Sasic et al. (2007), van der Schaaf et al. (2004) and Svensson et al. (1996)

Results of eight different flows are shown in table 1. It was possible to obtain the bubble length using PIV images for experiments I, II, V and VI. The sixth, sevenh and eigjhth columns of table 1 have mean bubble-velocity data measured using high-speed video camera, Eq. (3), and capacitive wire-mesh sensor together with PIV, Eq. (4), respectively. The results using both techniques are close, with differences lesser than 10 %. One can also see in Table 1

that using capacitive or resistive wire-mesh sensing gives almost the same result for the tests carried out in this work; the exception was the last flow case, for which the resistive technique gave higher velocities.

Table 1. Comparison of the results for bubble velocity.

Exp.	Water Flow Rate [L/min]	Water Superficial Velocity – J_w [m/s]	Air Flow Rate [L/min]	Air Superficial Velocity – J_a [m/s]	Velocity, by High Speed Video Camera [m/s]	Velocity, Wire-Mesh by Permittivity [m/s]	Velocity, Wire-Mesh by Conductivity [m/s]	Relative Error (%) HSVC x Permittivity	Relative Error (%) HSVC x Conductivity
I	180	0.187	35	0.036	0.91	0.88	0.88	2.9	3.2
II	180	0.187	39	0.041	0.91	0.93	0.92	1.9	1.2
III	180	0.187	46	0.048	1.016	- (*)	-	-	-
IV	180	0.187	51	0.053	1.049	-	-	-	-
V	240	0.249	32	0.033	0.95	0.92	0.98	3.0	3.0
VI	240	0.249	36	0.037	0.93	0.94	1.03	0.8	9.4
VII	240	0.249	45	0.047	1.027	-	-	-	-
VIII	240	0.249	52	0.054	1.105	-	-	-	-

(*) - Not measured with PIV, because the bubbles were larger than the visualization box.

5.1 AWMS and PIV synchronism

The synchronism of the AWMS with the PIV allowed the obtaining of tomographic images of a bubble passing over an axial section of the pipe and corresponding mean velocity profiles. Five velocity profiles were collected at the bubble zone and one at the slug zone. The cross-sectional and lateral images of the flow were taken with AWMS; the images give valuable qualitative information of the phenomenon during the bubble and the slug passage (Fig. 8).

The behavior of the velocity profiles, measured at the bottom of the annular duct at a diametrical vertical position, as a function of the bubble passage is quite interesting. In Fig. 8, the mean velocity decreases from the bubble nose to the bubble middle and then increases until the bubble tail. The minimum mean velocity (which is 0.017 m/s) occurs at position $5L_b/10$. Backflow is observed in some flows, depending on bubble size. The bigger the bubble, the more intense the back flow phenomenon. The AWMS images seen in Fig. 8 were obtained at 100 fps, using the Bruggeman model. Water fraction equal to one (only water at the crossing point) is represented with the color blue and air with green. In the axial image are illustrated 80 frames acquired in 0.8 s. One can observe the typical form of a bubble in annular duct flow, where the nose (at position $1L_b/10$) has a softer and rounder shape and the tail (at position $9L_b/10$) a sharper shape, occupying the top of the annular duct. Position $5L_b/10$ represents the middle of the bubble, which is the position where air occupies the most of the cross-sectional area. The synchronized PIV velocity-profile results at each of the five position of the bubble show that, as the bubble occupies a bigger region of the cross-section of the duct, the fluid beneath it decelerates.

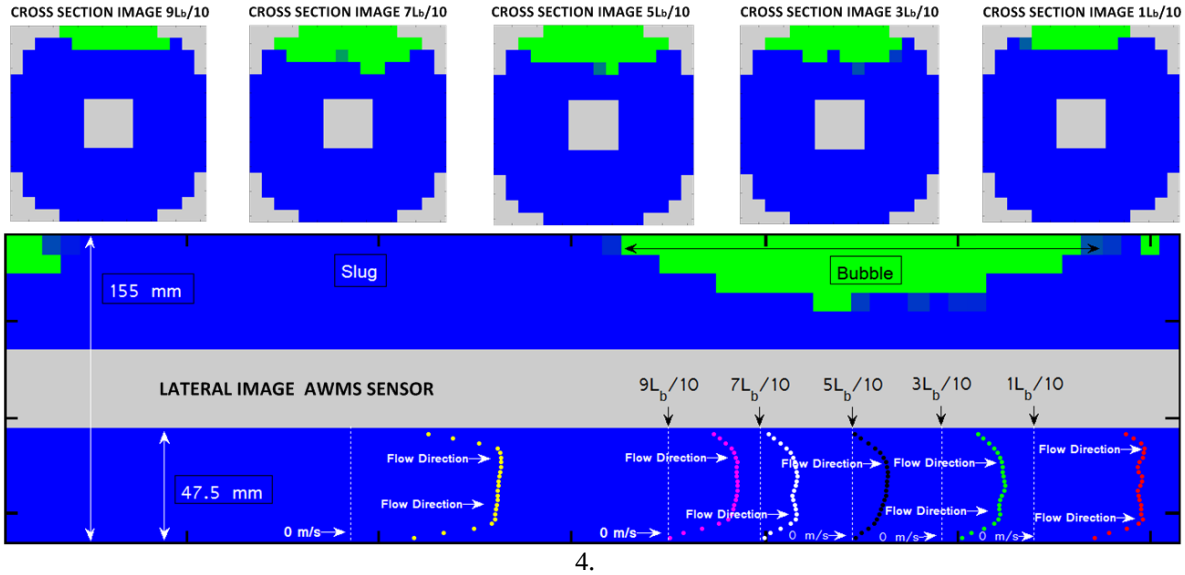

Figure 8. bubble crossing the visualization section at the top of the annular duct and mean axial velocity profiles at the bottom of the annular duct at different positions with respect to the bubble nose for jw = 0.187 [m/s] and ja = 0.041 [m/s].

6. CONCLUSIONS

Capacitive and resistive annular wire-mesh sensing were applied to study an air-water two-phase flow, arranged in the slug-flow pattern in an upward-5-degree-inclined concentric annular duct, with the help of high-speed video recording and particle image velocimetry (PIV). Void-fraction data as a function of time were collected, and with them the power spectral density (PSD) was calculated using Fast Fourier Transform (FFT). Dominant frequencies and peaks of power as a function of flow conditions were obtained: the higher the air flow rate, the lower the dominant bubble-passage frequency and the higher the power.

New bubble velocity data were obtained using two techniques: high-speed video camera and (capacitive and conductive) annular wire-mesh sensor together with PIV. From table 1, it can be seen an indication that: (i) bubble velocity increases as the water flow rate is increased, keeping the air flow rate approximately constant (see rows 1 and 4, for example), for both techniques presented; and (ii) bubble velocity increases as the air flow rate is increased, keeping the water flow rate constant. This is seen from the AWMS results (see experiments I and II or V and VI, for example). Using the high-speed video camera, this is seen when the air flow rate has a significant increase (over than 30%), in experiments I, III and IV; V, VII and VIII. When the increase is lower, the measurement error can be more important for some cases (I and II; V and VI) and show different results.

These results are not very conclusive yet, because both camera and AWMS recorded around 30 seconds, acquiring only 30 bubbles or fewer in some flows. The sensors were synchronized so they started recording at the same time, recorded for the same period and at the same sampling rate (100 Hz). In general, the two techniques obtained closer results, with differences less than 10%.

The synchronism of images showed the effects of the bubble passage on the flow beneath it. The velocity profiles suffer changes, so the mean velocities at each section also change: maximum velocity is observed at the nose, while the minimum is close to the middle. The slug velocity profile at the bottom region of the duct behaves almost as if it were single-phase water flow, not only in shape but also in magnitude, so it has higher values than those observed below the bubble. The slug velocity at the top side of the duct was not measured (the laser only illuminated the bottom region), but it is expected that the water travels faster, for the following reason: the water flow rate is constant over time. The only way to keep it constant is to have higher velocities at the top region of the duct. This difference in velocities may be explained analyzing the local pressure at each region: as the bubble passes, higher pressure is supposed to be measured at its nose, while lower pressure at its tail, causing higher velocities at the top region of the slug.

7. AKNOWLEDGEMENTS

The authors would like to thank STATOIL and ANP for the financial support and CNPq and FAPESP for the research grants.

8. REFERENCES

Belt, R.J., Van't Westende, J.M.C., Prasser, H.-M., Portela, L.M., 2010. Time and spatially resolved measurements of interfacial waves in vertical annular flow. INTERNATIONAL JOURNAL OF MULTIPHASE FLOW 36, 570–

Damsohn, M., Prasser, H.-M., 2009a. High-speed liquid film sensor with high spatial resolution. MEASUREMENT SCIENCE & TECHNOLOGY 20.

Damsohn, M., Prasser, H.-M., 2009b. High-speed liquid film sensor for two-phase flows with high spatial resolution based on electrical conductance. FLOW MEASUREMENT AND INSTRUMENTATION 20, 1–14.

Fulgosi, M., Lakehal, D., Banerjee, S., De Angelis, V., 2003. Direct numerical simulation of turbulence in a sheared airwater flow with a deformable interface. JOURNAL OF FLUID MECHANICS 482, 319–345.

Höhne, T., Kliem, S., Bieder, U., 2006. Modeling of a buoyancy-driven flow experiment at the ROCOM test facility using the CFD codes CFX-5 and Trio_U. NUCLEAR ENGINEERING AND DESIGN 236, 1309–1325.

Johnson, I.D., 1987. Method and apparatus for measuring water in crude oil. U.S. Patent 4664263.

Jones, O.C., Zuber, N., 1975. The interrelation between void fraction fluctuations and flow patterns in two-phase flow. INTERNATIONAL JOURNAL OF MULTIPHASE FLOW 2, 273–306.

Prasser, H.-M., Böttger, A., Zschau, J., 1998. A new electrode-mesh tomograph for gas-liquid flows. FLOW MEASUREMENT AND INSTRUMENTATION 9, 111–119.

Sasic, S., Leckner, B., Johnsson, F., 2007. Characterization of fluid dynamics of fluidized beds by analysis of pressure fluctuations. PROGRESS IN ENERGY AND COMBUSTION SCIENCE 33, 453–496.

Silva, M.J. Da, Schleicher, E., Hampel, U., 2007. Capacitance wire-mesh sensor for fast measurement of phase fraction distributions. MEASUREMENT SCIENCE AND TECHNOLOGY 18, 2245–2251.

Svensson, A., Johnsson, F., Leckner, B., 1996. Fluidization regimes in non-slugging fluidized beds: The influence of pressure drop across the air distributor. POWDER TECHNOLOGY 86, 299–312.

Takeda, Y., 1995. Velocity profile measurement by ultrasonic doppler method. EXPERIMENTAL THERMAL AND FLUID SCIENCE 10, 444–453.

van der Schaaf, J., van Ommen, J.R., Takens, F., Schouten, J.C., van den Bleek, C.M., 2004. Similarity between chaos analysis and frequency analysis of pressure fluctuations in fluidized beds. CHEMICAL ENGINEERING SCIENCE 59, 1829–1840.

Velasco Peña, H.F., Rodriguez, O.M.H., 2015. Applications of wire-mesh sensors in multiphase flows. FLOW MEASUREMENT AND INSTRUMENTATION 45, 255–273.

8. RESPONSIBILITY NOTICE

The authors are the only responsible for the printed material included in this paper.